JOURNAL OF THERMOPHYSICS AND HEAT TRANSFER
Vol. 22, No. 1, January–March 2008

Investigation of Hydrogen Droplet Solidification in Cryogenic Helium

Betul Unlusu,* Jinquan Xu,* and M. Yousuff Hussaini†
Florida State University, Tallahassee, Florida 32306
and
Dogan Celik‡ and Steven W. Van Sciver§
Florida State University, Tallahassee, Florida 32310

DOI: 10.2514/1.26858

Hydrogen-particle formation in liquid helium is investigated through a two-dimensional model. A liquid-hydrogen droplet at ∼14 K is injected into a helium bath of ∼4 K to produce a hydrogen particle. Hydrogen-particle formation in liquid helium involves vaporization of helium around the hydrogen droplet and its subsequent condensation, along with the simultaneous solidification of the droplet. To track the interface between the liquid and vapor phases of helium, the volume-of-fluid method is used. The enthalpy-porosity technique is employed to model hydrogen solidification. Numerical results are presented for the evolution of helium phase exchange and hydrogen solidification processes.

Nomenclature

A	=	source term in the momentum equation
$\boldsymbol{A}$	=	area vector, m^2
b	=	a small number introduced to the momentum equation to prevent division by zero
C	=	mushy zone constant
C_p	=	specific heat, J/kg K
$\boldsymbol{F}$	=	body force, N
$\boldsymbol{g}$	=	gravitational acceleration, m/s^2
h	=	sensible enthalpy, J/kg
k	=	thermal conductivity, W/mK
k_{eff}	=	effective conductivity, W/mK
L	=	latent heat, J/kg
N	=	number of cells
n	=	time step
$\boldsymbol{n}$	=	surface normal
p	=	pressure, Pa
q	=	heat flux at the interface, J/m^2 s
S_E	=	energy source term for the phase change of helium, J/m^3 s
S_h	=	energy source term for the solidification of hydrogen, J/m^3 s
S_L	=	mass source term, kg/m^3 s
T	=	temperature, K
T_{ref}	=	reference temperature, K
T_s	=	solidification temperature of hydrogen, K
t	=	time, s
V	=	control volume, m^3
$\boldsymbol{v}$	=	velocity, m/s
α	=	volume fraction
Γ_ϕ	=	diffusive source for ϕ
ΔH	=	nodal latent heat, J/kg
$\Delta \boldsymbol{s}$	=	displacement vector, m
ε	=	volume fraction of liquid hydrogen
κ	=	curvature
μ	=	viscosity, $N \cdot s/m^2$
ρ	=	density, kg/m^3
σ	=	coefficient of surface tension, N/m
ϕ	=	transport quantity

Subscripts

f	=	cell faces
L	=	liquid
L/S_{hydrogen}	=	liquid or solid hydrogen side of the hydrogen–helium interface
S	=	solid
V	=	vapor
V_{helium}	=	helium vapor side of the hydrogen–helium interface

Presented as Paper 4550 at the 41st AIAA/ASME/SAE/ASEE Joint Propulsion Conference and Exhibit, Tucson, AZ, 10–13 July 2005; received 28 July 2006; revision received 11 June 2007; accepted for publication 13 June 2007.

*Postdoctoral Research Fellow, School of Computational Science, 400 Dirac Science Library. Member AIAA.

†Sir James Lighthill Professor of Mathematics and Computational Science and Engineering, School of Computational Science.

‡Research Fellow, Magnet Science and Technology, National High Magnetic Field Laboratory.

§Professor, Magnet Science and Technology, National High Magnetic Field Laboratory.

I. Introduction

ATOMIC propellants such as boron, carbon, or hydrogen stored in solid matrices at cryogenic temperatures have been of significant interest for decades, due to their ability to provide high specific impulse [600–1300 s for 10% atomic hydrogen in solid-hydrogen/liquid-helium (SH_2/LHe) systems]. The atoms are isolated from one another and stabilized in the solid matrix. Recombination of atoms takes place upon heating and results in high energy release and rapid acceleration [1–4]. Hydrogen particles are desirable as the solid matrix because low-density matrices are needed to increase the energy output of the propellant system. Trapping of impurity atoms in solid hydrogen has been examined using electronic spectroscopy in several studies [5,6]. Numerical simulations have also been carried out to analyze the stability of the matrix-impurity system at different impurity concentrations [7,8].

Atomic propellant feed systems require the production, storage, and transport of solid-hydrogen particles in cryogenic fluids. Formation of hydrogen particles in helium has been experimentally investigated for years [1–4]. In a recent study [9], hydrogen particles with diameters of 1 to 6.4 mm were produced in liquid helium. Immediate solidification followed by the agglomeration of particles was observed via video imaging. Particle formation efficiencies were

also determined. Theoretical and computational investigations of a hydrogen-particle/liquid-helium slurry piping system were recently conducted with a view to maximize hydrogen loading and facilitate particle transportation [10]. For production of solid-hydrogen particles, a direct-injection technology has been developed [11]. In this process, a droplet of liquid hydrogen at ∼14 K is introduced from a vibrating orifice to a system containing liquid helium at ∼4 K. Complex energy-exchange processes between the two fluids results in the vaporization of helium around the hydrogen droplet and its subsequent condensation (boiling point of 4.2 K) and in the simultaneous solidification of the liquid-hydrogen droplet (solidification point of 13.8 K). In the early stages of the process, as hydrogen cools down to the solidification temperature, a small amount of helium vaporizes around it. During solidification, the heat transferred from hydrogen to helium is balanced by the heat of fusion and the temperature of the hydrogen droplet stays constant. After solidification is complete, as the temperature of the hydrogen droplet approaches the temperature of the bath, vaporization around the droplet slows and condensation of helium becomes prominent.

With the objective of understanding the process of solid-hydrogen-particle generation, a series of numerical experiments have been conducted to investigate helium phase exchange and hydrogen solidification [12]. In these simulations, the solidification of hydrogen and vaporization/condensation of helium are studied in isolation. To study the vaporization/condensation processes in isolation, it is assumed that the shape and size of the droplet remain constant and that the temperature evolution at the interface between helium and hydrogen has a linear profile in time. Solidification of the droplet is studied in isolation by keeping the outermost droplet boundary at the liquid-helium temperature, thereby neglecting the vaporization/condensation process. These restrictions are relaxed in the present study, which couples the hydrogen solidification and helium vaporization/recondensation processes.

The governing equations are the two-dimensional unsteady multiphase incompressible Navier–Stokes equations with appropriate source terms in the equations of continuity and energy to account for mass and heat generation, respectively, due to phase exchange. The momentum equation includes a force term that represents surface tension at the interface between liquid and vapor phases. These equations are solved by the so-called semi-implicit pressure-linked equation (SIMPLE) method [13].

II. Physical Model and Parameters

Figure 1 shows the prototype system. The helium bath has a width of 4 mm and a height of 8 mm. For simplicity, we assume that the hydrogen droplet with a diameter of 1 mm is introduced at the center of the domain, in which it remains static.

A. Vaporization and Condensation of Helium

The following continuity equation is solved for the volume fraction of liquid helium. The volume fraction of helium vapor is determined from the volume fraction balance:

$$\frac{\partial \alpha_L}{\partial \mathrm{t}} + \boldsymbol{v} \cdot \nabla \alpha_L = \frac{S_L}{\rho_L} \tag{1}$$

where S_L is the source term defined as

$$S_L = \frac{(q_V - q_L)\nabla \alpha_L}{L} \tag{2}$$

The difference between the heat fluxes on the vapor and liquid sides is approximated by the following equation:

$$q_V - q_L = -\frac{\underbrace{(k_L \alpha_L + k_V \alpha_V)}\nabla T}{k_{\text{eff}}} \tag{3}$$

In Eq. (3), the term in the parentheses is also known as the effective thermal conductivity k_{eff}.

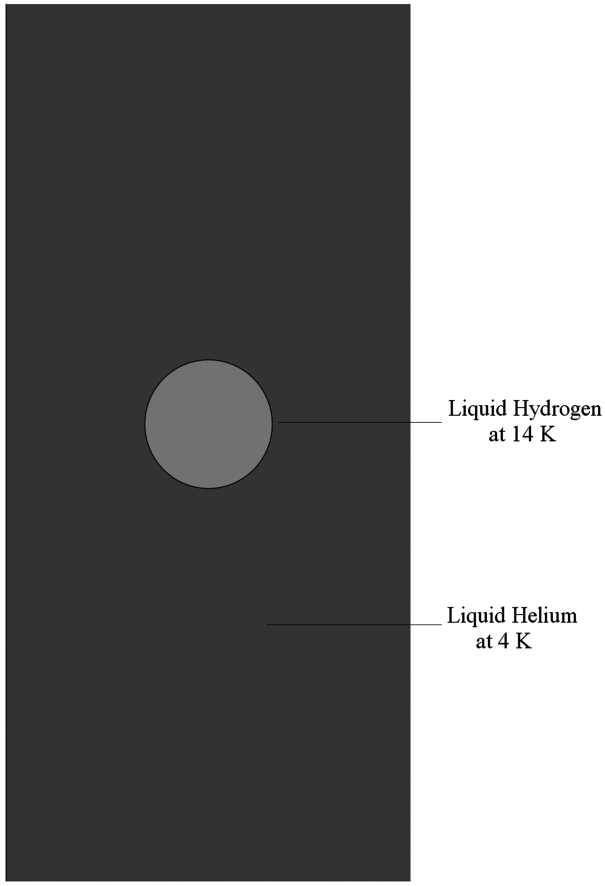

Fig. 1 Prototype system.

A single momentum equation is solved for the velocity field associated with both liquid and vapor phases:

$$\frac{\partial}{\partial t}(\rho \boldsymbol{v}) + \nabla \cdot (\rho \boldsymbol{v}\boldsymbol{v}) = -\nabla \mathrm{p} + \nabla \cdot [\mu(\nabla \boldsymbol{v} + \nabla \boldsymbol{v}^T)] + \rho \boldsymbol{g} + \boldsymbol{F} \tag{4}$$

where density ρ and viscosity μ are defined (based on volume fractions) in each control volume:

$$\rho = \rho_L \alpha_L + \rho_V \alpha_V, \qquad \mu = \mu_L \alpha_L + \mu_V \alpha_V \tag{5}$$

In Eq. (4), the source term $\boldsymbol{F}$ models the effect of surface tension, which is defined as

$$\boldsymbol{F} = \sigma_{LV} \frac{\rho \kappa_L \nabla \alpha_L}{\frac{1}{2}(\rho_L + \rho_V)} \tag{6}$$

The curvature κ_L is defined in terms of the surface normal $\boldsymbol{n}$:

$$\boldsymbol{n} = \nabla \alpha_L \qquad \kappa_L = \nabla \cdot \frac{\boldsymbol{n}}{|n|} \tag{7}$$

Similarly, a single energy equation is solved for the two phases:

$$\frac{\partial}{\partial t}(\rho h) + \nabla \cdot (\rho h \boldsymbol{v}) = \nabla \cdot (k_{\text{eff}} \nabla T) + S_E \tag{8}$$

where sensible enthalpy h, temperature T, and the source term S_E are defined as

$$h = \frac{h_L \rho_L \alpha_L + h_V \rho_V \alpha_V}{\rho_L \alpha_L + \rho_V \alpha_V}, \qquad T = \frac{T_L \rho_L \alpha_L + T_V \rho_V \alpha_V}{\rho_L \alpha_L + \rho_V \alpha_V} \tag{9}$$

and

$$S_E = L S_L \tag{10}$$

In Eq. (9), h_V is defined as

Table 1 Physical parameters of helium and hydrogen

	Helium (liquid)	Helium (vapor)	Hydrogen (solid)	Hydrogen (liquid)
Density, kg/m^3	125.4	16.5	92	71
Thermal conductivity, W/mK	0.0186	0.009	1	0.1
Viscosity, $\times 10^5$ Pa · s	0.318	0.124		1.36
Specific heat, J/kg · K	5170	9033	2700	9500
Latent heat, J/kg	21000		60000	

Table 2 Thermal properties of helium vapor

Temperature, K	Thermal conductivity, W/mK	Specific heat, J/kg K
4.2	0.009	9033
6.0	0.012	6011
8.0	0.015	5575
10.0	0.017	5426
12.0	0.019	5353
14.0	0.021	5310

$$h_V = \int_{T_{\text{ref}}}^{T} C_{pV}\,\mathrm{d}T \tag{11}$$

A constant value for the specific heat of liquid helium, C_{pL}, is used in the calculations (see Table 1). Temperature-dependent values of C_{pV} are presented in Table 2.

The volume-of-fluid method [14] is used to track the interface between the liquid and vapor helium. If the volume fractions of fluids in a given cell are between zero and one, the cell contains the interface. This method assumes that the moving interface has a linear slope in each cell and uses the values of the volume fractions and their derivatives to reconstruct the interface [15]. The position of the interface is calculated relative to the center of each partially filled cell. After an approximation to the interface is calculated, the amount of fluid that is advected through each face is determined. This is followed by calculating the new volume fractions using a flux balance.

B. Solidification of Hydrogen

We model the solidification of hydrogen using the enthalpy-porosity method [16–18]. The main idea behind this method is to introduce the latent heat as a source term in the energy equation:

$$\frac{\partial h}{\partial t} + \nabla \cdot (\boldsymbol{v}h) = \frac{k}{\rho}(\nabla^2 T) + \frac{S_h}{\rho} \tag{12}$$

As a first approximation, density ρ is assumed to be the average of the solid and liquid densities, and k is taken as the thermal conductivity of the solid phase.

The phase change is an isothermal process, and the source term is defined as

$$\frac{S_h}{\rho} = \frac{\partial(\Delta H)}{\partial t} \tag{13}$$

where ΔH is a step function of temperature:

$$\Delta H = \begin{cases} 0, & \text{if } T < T_s \\ L, & \text{if } T > T_s \end{cases} \tag{14}$$

In the case of an isothermal phase change, the interface between the liquid and the solid phases is sharp. The enthalpy-porosity model is particularly suitable for situations in which solidification/melting occurs only in part of the domain discretized with a fixed grid. For each computational cell, a latent heat value is calculated using cell temperatures. The volume fractions in cells undergoing phase change are then determined using the assigned latent heat values.

A single momentum equation is solved for liquid and solid hydrogen:

$$\frac{\partial \boldsymbol{v}}{\partial \mathrm{t}} + \boldsymbol{v} \cdot \nabla \boldsymbol{v} = \frac{\mu}{\rho}\nabla^2 \boldsymbol{v} + \boldsymbol{g} - \frac{\nabla p}{\rho} + \frac{A\boldsymbol{v}}{\rho} \tag{15}$$

In this equation, A is defined as

$$A = -C\frac{(1-\varepsilon)^2}{\varepsilon^3 + b} \tag{16}$$

where C is on the order of 10^5. In cells containing only liquid, A is zero and does not have any effect on the velocity field. On the other hand, in cells containing only solid, a large value of A will ensure that the velocities are equal to zero. The source term in the momentum equation ensures that the velocities are equal to zero in the solid phase [16].

The equation of continuity is solved, along with the momentum and energy equations:

$$\nabla \cdot \boldsymbol{v} = 0 \tag{17}$$

The present study examines the two phase-change processes as a conjugate problem by taking the thermal coupling of the hydrogen droplet with the helium tank into account.

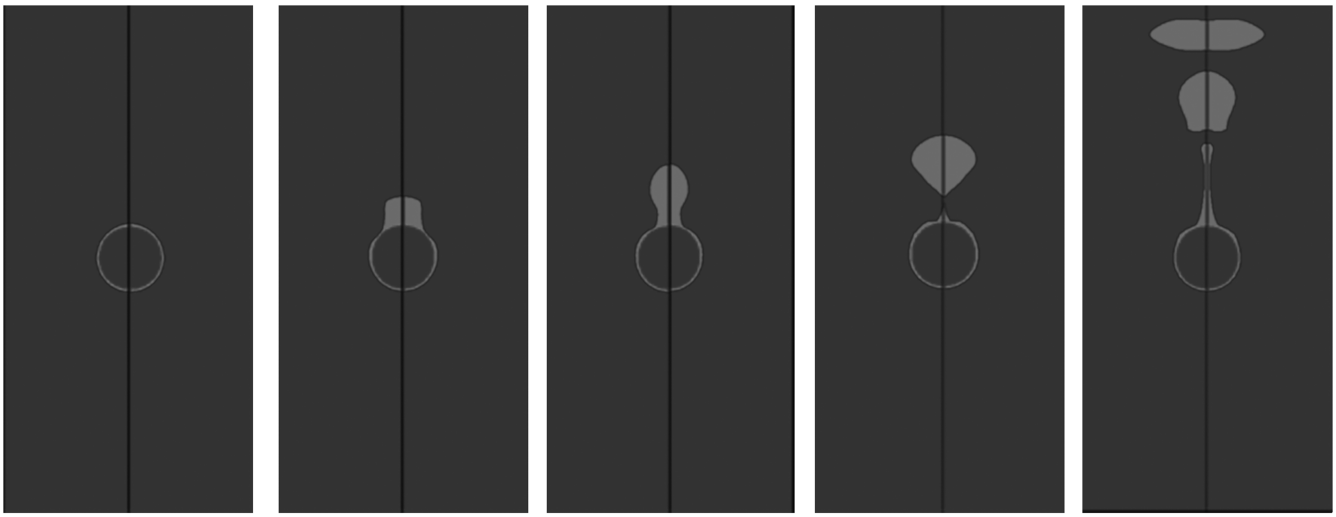

Fig. 2 Evolution of the vapor-liquid interface.

C. Thermal Coupling of a Hydrogen Droplet with a Helium Tank

At the interface between the hydrogen droplet and vapor helium, the temperature and the heat flux are continuous.

$$T_{V\,\text{helium}} = T_{L/S\,\text{hydrogen}}, \qquad (q_{V\,\text{helium}} - q_{L/S\,\text{hydrogen}}) \cdot \boldsymbol{n} = 0 \quad (18)$$

In the solution procedure, the temperature of each cell is calculated using the energy equations and thermal coupling at the hydrogen–helium interface. If the temperature predicted by the energy equation for any hydrogen cells is lower than the solidification temperature, the source term based on the enthalpy of fusion extinguishes this difference. Therefore, any cell containing both liquid and solid phases will be at the phase-change temperature.

D. Model Parameters

Table 1 shows the physical parameters used in the present study. These parameters are obtained at the saturation temperature and pressure of helium and hydrogen [19,20].

In the temperature range of interest, the thermal conductivity and specific heat of helium vapor change significantly. Therefore, temperature-dependent values are used for these parameters (see Table 2).

E. Solution Technique

The governing equations are solved using an unstructured grid with 40,190 quadrilateral elements. Exploiting the symmetry of the problem, the equations are solved for only half of the domain. The left boundary is a symmetry boundary, in which the normal component of velocity and normal gradients of all variables are equal to zero. The top boundary is open, with a specified temperature of 4 K. The no-slip condition is enforced at the right and bottom boundaries, which are also maintained at 4 K.

A finite volume technique is used for the solution of the governing equations, which are cast in the generic integral form [14]:

$$\int_V \frac{\partial \rho\phi}{\partial t}\,\mathrm{d}V + \oint \rho\phi\boldsymbol{v}\cdot\mathrm{d}\boldsymbol{A} = \oint \Gamma_\phi \nabla\phi\cdot\mathrm{d}\boldsymbol{A} + \int_V \mathrm{S}_\phi\,\mathrm{dV} \quad (19)$$

In the continuity equation, ϕ equals unity. In the momentum and energy equations, ϕ represents the velocity vector and sensible enthalpy, respectively.

The implicit Euler method is used for the time discretization of Eq. (19):

$$\frac{(\rho\phi\mathrm{V})^{n+1} - (\rho\phi\mathrm{V})^{n}}{\Delta\mathrm{t}} + \sum_f^{N_f} \rho_f^{n+1}\boldsymbol{v}_f^{n+1}\phi_f^{n+1}\cdot\boldsymbol{A}_f = \sum_f^{N_f} \Gamma_\phi^{n+1}(\nabla\phi)^{n+1}\cdot\boldsymbol{A}_f + \mathrm{S}_\phi^{n+1}\mathrm{V} \quad (20)$$

The discreet values of the transport quantity ϕ are stored at the cell centers. The second-order upwind scheme is used for the calculation of the quantities at cell faces ϕ_f:

$$\phi_f = \phi + \nabla\phi\cdot\Delta\boldsymbol{s} \quad (21)$$

where ϕ is the cell-centered value, and $\Delta\boldsymbol{s}$is calculated from the upstream cell centroid to the face centroid. The gradient $\nabla\phi$ is calculated as

$$\nabla\phi = \frac{1}{\mathrm{V}}\sum_f^{N_f} \tilde{\phi}_f\boldsymbol{A} \quad (22)$$

In Eq. (22), the face values $\tilde{\phi}_f$ are obtained from averaging the cell-centered values adjacent to the face.

The discrete continuity, momentum, and energy equations in the form of Eq. (20) are solved sequentially using the Gauss–Seidel method. The momentum equations are solved first, and the velocity field obtained is corrected using the pressure-correction equation derived from the continuity equation. The semi-implicit method for pressure-linked equations (SIMPLE) is used to introduce pressure into the continuity equation [13]. Finally, the energy equation is solved.

The time scale of the boiling process is on the order of milliseconds, and time steps as low as 10^{-5} s are used in the simulation. The convergence criterion is that the scaled residuals for all equations, except the energy equation, should be less than 10^{-3}. The criterion is 10^{-6} for the energy equation.

III. Results and Discussion

We simulate the formation of hydrogen particles in helium in two dimensions and study the evolution of the liquid-vapor and liquid-solid interfaces, as well as the temperature and velocity fields. The half-domain results are reflected across the left symmetry boundary and presented in the full domain.

A. Phase Change of Helium

Phase change of helium can take place through nucleate or film-boiling mechanisms during thermal equilibration. Compared with nucleate boiling, film boiling requires a higher temperature difference between the hot and cold media to start. In film boiling, a thin, continuous vapor film forms around the hot medium and separates it from the liquid until the wall fluxes drop below the minimum film-boiling heat flux. After that point, the film collapses, and eventually boiling takes place at only distinct spots (nucleate boiling). In our case, the initial temperature of the hydrogen droplet is sufficiently high to start film boiling. We determine that the initial wall flux is higher than the maximum nucleate boiling heat flux ($\sim$0.5–0.85 W/cm^2) [21]. In addition, until the end of the solidification process, wall heat fluxes do not drop to the minimum film-boiling heat flux ($\sim$0.35 W/cm^2) [21]. In our simulations, we observe that a stable vapor film with a thickness of about 0.04 mm covers the droplet, and the liquid does not contact with the hot wall until the solidification of the hydrogen droplet is completed.

Figure 2 shows the evolution of helium vapor around the hydrogen droplet. Initially, there is a vapor film of uniform thickness around the droplet. As a result of vaporization, the thickness of the film increases. Because of buoyancy forces, vapor moves up, and a neck emerges at the top of the droplet. Eventually, a bubble forms and pinches off. The growth and departure process takes about 35 ms. Another bubble begins to form as the detached bubble rises in the bath [22,23].

Figure 3 shows the temperature contours in the bath corresponding to each frame in Fig. 2. We started with an initial temperature profile that increases from the saturation temperature at the liquid-vapor interface to the temperature of the hot droplet. The liquid-vapor interface can be observed in the temperature contours. Also, as expected, the temperature of the bubble decreases as it moves away from the droplet. The temperature of the droplet, on the other hand, stays constant during solidification.

Figure 4 shows the velocity profiles at an elapsed time of 35 ms. The right-hand side of the figure shows the velocity profiles in each phase and the left-hand side shows the magnitudes. We observe that the vapor formed around the lower portion of the droplet rapidly migrates to the upper portion. The velocity profile displays the movement of the bubble in the vertical direction as well as the change in the bubble shape in the horizontal direction. The bubble eventually becomes ellipsoidal (see Fig. 2). The liquid being pushed away by the rising bubble and the liquid flow beneath the bubble to fill up the emptied space can both be observed. The maximum velocity is found to be about 0.3 m/s.

B. Solidification of Hydrogen

The initial temperature of the droplet is just above the solidification point. Upon contact with helium, the outer layer of the droplet immediately cools to the solidification temperature and phase change begins. Solidification is an exothermic process, and the heat expelled has to be taken away for the phase change to proceed. The heat of fusion per kilogram of hydrogen is almost three times higher

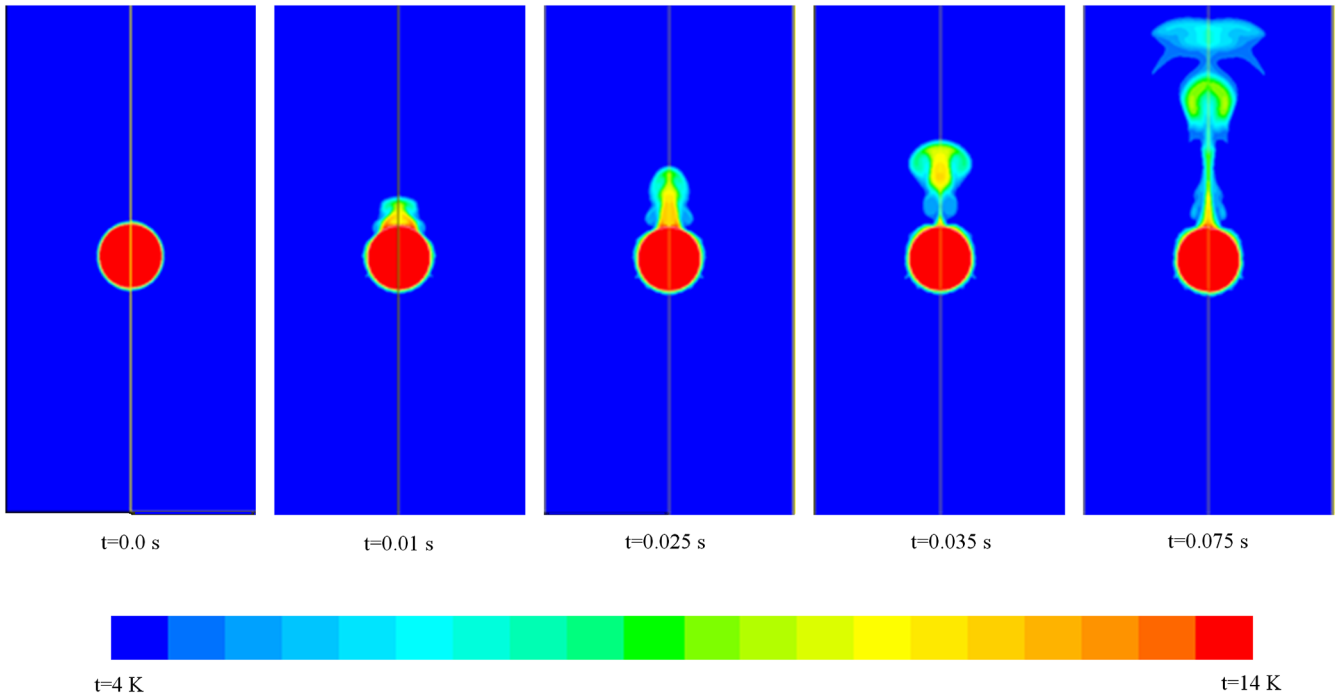

Fig. 3 Temperature contours in the bath.

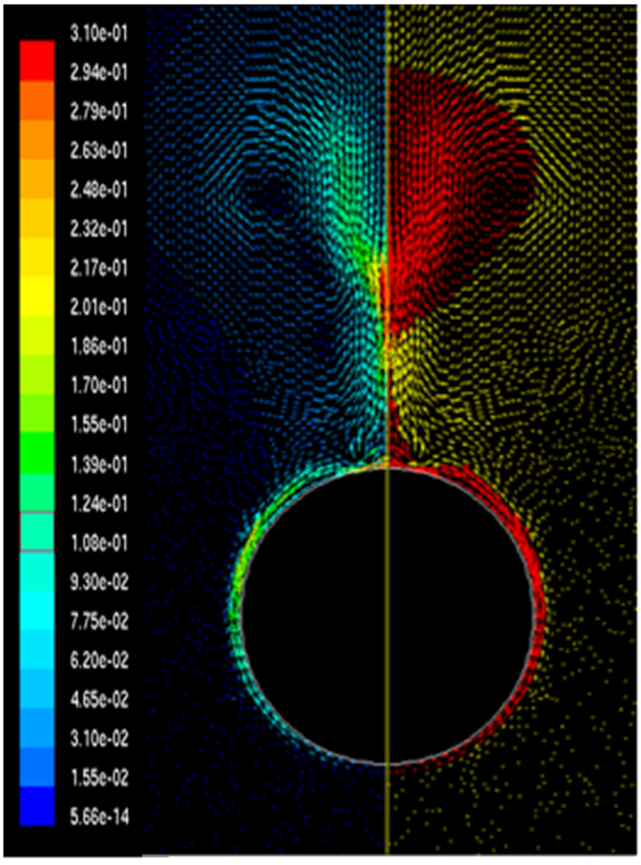

Fig. 4 Flowfield in the bath at $t = 0.035$ s.

than the heat of vaporization of helium, and a significant amount of energy must be transferred from hydrogen to helium for solidification to be completed. On the other hand, time steps are as small as 10^{-5} s, and therefore the simulation of the coupled process is computationally expensive.

Figure 5 shows the phase fronts during solidification. At the very beginning of the process, the fronts are circular, which is similar to the case in which the solidification of the hydrogen droplet is decoupled from the vaporization of helium. In the noncoupled simulations conducted by Xu et al. [12], the initial temperature of the hydrogen droplet was 20 K. In the present study, the initial temperature is selected as 14 K, (which is just above the freezing point) to enable comparison with some experimental studies [3,9] and to reduce computational cost. We have run noncoupled simulations with the new initial temperature to compare with the current results (see Fig. 6a for the solidification front and the temperature contours when the two phase-change processes are not coupled). In the coupled simulation, the shape of the phase fronts does not stay perfectly circular at later times, because during the process, the vapor layer around the upper portion of the droplet gets thicker, heat transfer slows, and phase change progresses relatively slower. We observe that the droplet freezes in about 0.5 s.

Figure 6b shows the change in the solidification times at three different heats of solidification (5000, 20,000, and 60,000 J/kg) for cases in which the two phase-change processes are coupled and not coupled. The solidification time and its dependence on the heat of solidification are higher in the case of coupled simulations due to the heat-transfer resistance caused by the vapor film around the droplet. Note that the temperature of the outer layer of the droplet is kept constant at 4 K in the simulation of the solidification process when decoupled from the boiling of helium.

The temperature contours during solidification are presented in Fig. 7. When solidification is in progress, the temperature of the solidified part decreases very slowly. After 0.49 s, when solidification has just been completed, the minimum temperature drops to around 11 K. At this time, film boiling is still the phase-change mechanism (see Fig. 8). Afterward, the temperature of the droplet decreases quickly. We determine that the vapor film around the droplet collapses at an elapsed time of 0.54 s, when the average temperature of the droplet is about 10 K.

IV. Conclusions

We reached the following conclusions through the two-dimensional simulation of the formation of hydrogen particles in liquid helium.

1) Coupled simulation of the vaporization/condensation and solidification processes is computationally intensive due to the range of time and spatial scales.

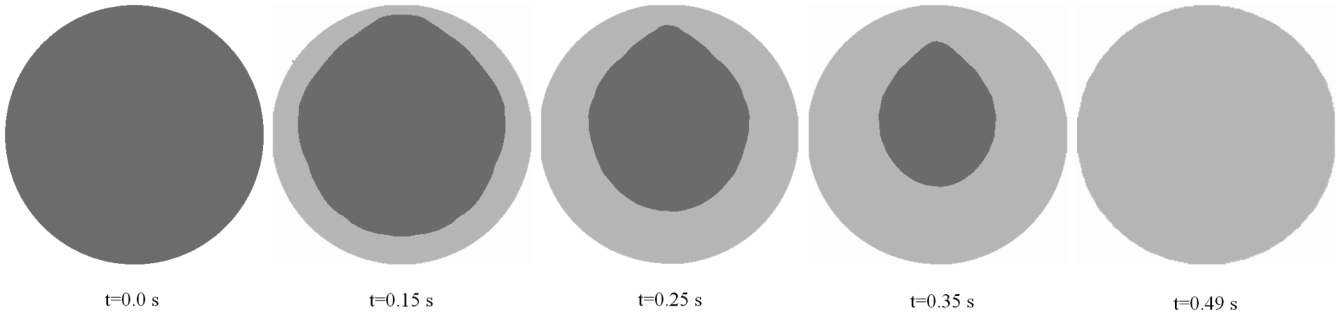

Fig. 5 Evolution of solidification.

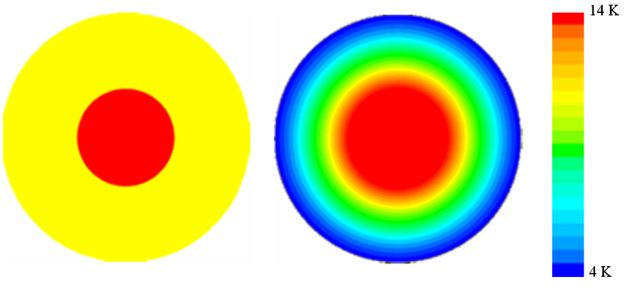

a)

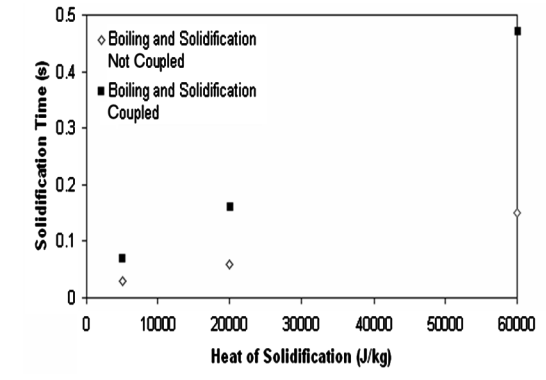

b)

Fig. 6 Shown are a) the solidification front and the associated temperature contours for the case in which the solidification of the hydrogen droplet is decoupled from the boiling of helium and b) the change in the solidification time with the heat of solidification.

2) Solidification of a hydrogen droplet begins immediately upon contact with helium. When the solidification process is coupled with the boiling of helium, the phase fronts do not stay perfectly circular, because the upper portion of the droplet freezes slower and the heat transfer is slower, due to the vapor layer being thicker here. It takes about 0.5 s for a hydrogen droplet with a diameter of 1 mm to solidify.

3) The solidification time obtained in coupled simulations of the two phase-change processes is higher than that obtained in the isolated solidification simulation, due to the heat-transfer resistance caused by the vapor film in the former case.

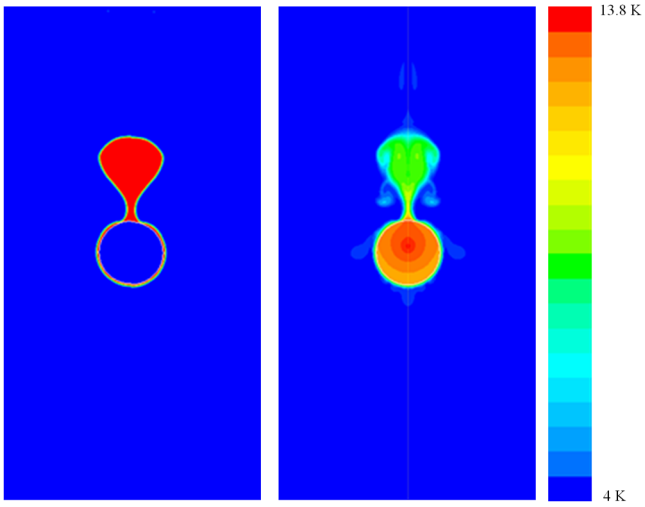

Fig. 8 Liquid-vapor phase front and temperature contours in the bath at $t = 0.49s$.

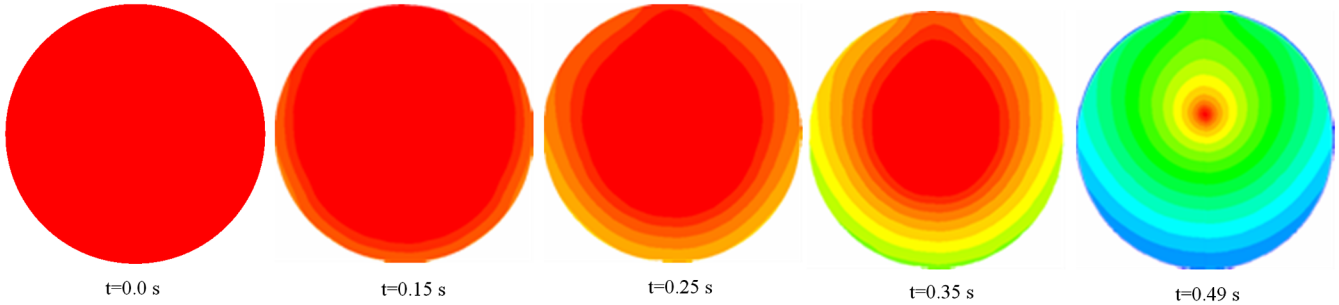

Fig. 7 Temperature contours within the hydrogen droplet.

The results obtained in this study are comparable with experiments [1–4] in which solid-hydrogen particles immediately emerge after the droplets come into contact with helium. For a better understanding of the process, multiple hydrogen droplets, their interactions with each other, and their motion in the helium bath should be examined.

Acknowledgments

This work was partially supported by the NASA Hydrogen Research Program for Florida Universities (contract no. NAG3-2751) and the Office of the Provost at Florida State University.

References

[1] Palaszewski, B., "Atomic Hydrogen as a Launch Vehicle Propellant," NASA TM-102459, 1990.

[2] Palaszewski, B., "Launch Vehicle Performance with Solid Particle Feed Systems for Atomic Propellants," NASA TM-208498, 1998.

[3] Palaszewski, B., "Solid Hydrogen Experiments for Atomic Propellants," NASA TM-211292, 2001.

[4] Palaszewski, B., "Solid Hydrogen Experiments for Atomic Propellants: Image Analysis," NASA TM-211297, 2002.

[5] Fajardo, M. E., "Matrix Isolation Spectroscopy of Metal Atoms Generated by Laser Ablation, 2: The Li/Ne, Li/D2 and Li/H2 Systems," *Journal of Chemical Physics*, Vol. 98, No. 1, 1993, pp. 110–118.
doi:10.1063/1.464659

[6] Fajardo, M. E., Tam, S., Thomson, T. L., and Cordonnier, M. E., "Electronic Spectroscopy of B Atoms and B2 Molecules Isolated in Para-H, Normal D, Ne, Ar, Kr, and Xe Matrices," *Journal of Chemical Physics*, Vol. 113, No. 20, 2000, pp. 9067–9078.
doi:10.1063/1.1312268

[7] Krumrine, J. R., Jang, S., Alexander, M. H., and Voth, G. A., "Quantum Molecular Dynamics and Spectral Simulation of a Boron Impurity in Solid Para-Hydrogen," *Journal of Chemical Physics*, Vol. 113, No. 20, 2000, pp. 9079–9089.
doi:10.1063/1.1318225

[8] Mirijanian, D. T., Alexander, M. H., and Voth, G. A., "Path Integral Molecular Dynamics Simulation of Solid Para-Hydrogen with an Aluminum Impurity," *Chemical Physics Letters*, Vol. 365, No. 5, 2002, pp. 487–493.
doi:10.1016/S0009-2614(02)01505-1

[9] Palaszewski, B., "Solid Hydrogen Experiments for Atomic Propellants: Particle Formation Energy and Imaging Analyses," NASA TM-211915, 2002.

[10] Xu, J., Rouelle, A., Smith, K. M., Celik, D., Hussaini, M. Y., and Van Sciver, S. W., "Two-Phase Flow of Solid Hydrogen Particles and Liquid Helium," *Cryogenics*, Vol. 44, No. 6, 2004, pp. 459–466.
doi:10.1016/j.cryogenics.2004.02.008

[11] Xu, J., Hussaini, M. Y., Celik, D., and Van Sciver, S. W., "Numerical Study of Liquid Hydrogen Droplet Generation from a Vibrating Orifice," *Physics of Fluids*, Vol. 17, No. 8, 2005, pp. 082103–082103-8.
doi:10.1063/1.1946767

[12] Xu, J., Smith, K. M., Celik, D., Hussaini, M. Y., and Van Sciver, S. W., "Hydrogen Particles in Liquid Helium," *Cryogenics*, Vol. 44, No. 6, 2004, pp. 507–514.
doi:10.1016/j.cryogenics.2004.02.017

[13] Patankar, S. V., *Numerical Heat Transfer and Fluid Flow*, McGraw–-Hill, New York, 1980, Chap. 6.

[14] Puckett, E. G., Almgren A. S., Bell, J. B., Marcus, D. L., and Rider W. J., "A High-Order Projection Method for Tracking Fluid Interfaces in Variable Density Incompressible Flows," *Journal of Computational Physics*, Vol. 130, No. 2, 1997, pp. 269–282.
doi:10.1006/jcph.1996.5590

[15] Youngs, D. L., "Time Dependent Multi-Material Flow with Large Fluid Distortion," *Numerical Methods for Fluid Dynamics*, edited by K. W. Morton, Academic Press, New York, 1982.

[16] Voller, V. R., and Prakash, C., "A Fixed-Grid Numerical Modeling for Convection Diffusion Mushy Region Phase-Change Problems,"*International Journal of Heat and Mass Transfer*, Vol. 30, No. 8, 1987, pp. 1709–1720.
doi:10.1016/0017-9310(87)90317-6

[17] Voller, V. R., and Swaminathan, C. R., "General Source-Based Method for Solidification Phase Change," *Numerical Heat Transfer, Part B, Fundamentals*, Vol. 19, No. 2, 1991, pp. 175–189.
doi:10.1080/10407799108944962

[18] Brent, A. D., Voller, V. R., and Reid, K. J., "Enthalpy-Porosity Technique for Modeling Convection-Diffusion Phase-Change: Application to the Melting of a Pure Metal," *Numerical Heat Transfer*, Vol. 13, No. 3, 1988, pp. 297–318.
doi:10.1080/10407788808913615

[19] Anon., "NIST Chemistry WebBook," *NIST Standard Reference Database Number 69* [online database], http://webbook.nist.gov/chemistry/ [cited 27 June 2005].

[20] Souers, P. C., *Hydrogen Properties for Fusion Energy*, Univ. of California Press, Berkeley, CA, 1986, Chaps. 5, 6.

[21] Van Sciver, S. W., *Helium Cryogenics*, Plenum, New York, 1986, Chap. 6.

[22] Welch, S. W. J., and Wilson, J., "A Volume of Fluid Based Method for Fluid Flows with Phase Change," *Journal of Computational Physics*, Vol. 160, No. 2, 2000, pp. 662–682.
doi:10.1006/jcph.2000.6481

[23] Juric, D., and Tryggvason, G., "Computations of Boiling Flows," *International Journal of Multiphase Flow*, Vol. 24, No. 3, 1998, pp. 387–410.
doi:10.1016/S0301-9322(97)00050-5